JOURNAL OF GEOPHYSICAL RESEARCH, VOL. 115, B04302, doi:10.1029/2009JB006678, 2010

Seafloor topography, ocean infragravity waves, and background Love and Rayleigh waves

Yoshio Fukao,[1] Kiwamu Nishida,[2] and Naoki Kobayashi[3]

Received 27 April 2009; revised 4 October 2009; accepted 28 October 2009; published 2 April 2010.

[1] We propose that background Love and Rayleigh waves in a frequency range 5–20 mHz are generated primarily by ocean infragravity waves in the same frequency range by a linear coupling process with seafloor topography. Wavelengths of infragravity waves in this frequency range are on the order of 10 to 40 km in the deep ocean. The seafloor topography with wavelengths of this order is dominated by abyssal hills, which are the most widespread physiographic forms on Earth, covering as much as 85% of the Pacific floor. Interaction of infragravity waves in the deep ocean with these hills generates a random distribution of point-like tangential forces on the seafloor which may be large enough to excite Love and Rayleigh waves simultaneously. We quantify this idea by using the known statistical property of hills distribution in the Pacific and by noting that heights of abyssal hills are an order of magnitude smaller than depths of the deep ocean, so that the topography-related phase velocity change can be neglected. The model is reasonably consistent with the Love to Rayleigh wave amplitude ratio reported at 10–20 mHz and the observed background Rayleigh wave spectrum with a characteristic plateau around 8 mHz. Contribution of topographic coupling in shallow, coastal seas is not included in our simple model but should be important, especially at frequencies above 20 mHz.

Citation: Fukao, Y., K. Nishida, and N. Kobayashi (2010), Seafloor topography, ocean infragravity waves, and background Love and Rayleigh waves, *J. Geophys. Res.*, *115*, B04302, doi:10.1029/2009JB006678.

1. Introduction

[2] The solid Earth is incessantly shaken by near-surface random disturbances, a phenomenon called Earth's background free oscillations or Earth's hum [*Nawa et al.*, 1998; *Suda et al.*, 1998; *Kobayashi and Nishida*, 1998; *Tanimoto et al.*, 1998]. Their intensities are variable annually and semiannually [*Nishida et al.*, 2000; *Tanimoto*, 2001; *Ekström*, 2001] and spatially on a Pacific scale [*Rhie and Romanowicz*, 2004; *Nishida and Fukao*, 2007]. This phenomenon defines the lowest level of ground noise in the seismic passband 2–20 mHz [*Nishida et al.*, 2002]. There is little doubt that the excitation sources lie in the atmosphere or oceans or both. In either case, the atmospheric kinetic energy powered by solar irradiation is the major source of the "hum." Several excitation mechanisms of either direct (atmospheric) [*Kobayashi and Nishida*, 1998; *Fukao et al.*, 2002] or indirect (oceanic) [*Watada and Masters*, 2001; *Rhie and Romanowicz*, 2004; *Tanimoto*, 2005, 2007; *Webb*, 2007, 2008] origin have been proposed on the basis of the observations of background spheroidal oscillations (or Rayleigh waves). Regardless of whether the excitation sources are in the atmosphere or oceans, the mechanisms so far proposed assume that background free oscillations are generated by pressure forces vertically acting on Earth's surface horizon, which should preferentially excite spheroidal oscillations and poorly generate toroidal oscillations. The most recent analyses of horizontal seismograms, however, have revealed generation of background toroidal oscillations with amplitudes as large as spheroidal oscillations [*Kurrle and Widmer-Schnidrig*, 2008] or Love waves with kinetic energies as large as Rayleigh waves [*Nishida et al.*, 2008], a phenomenon that cannot be explained by any models so far proposed. Here we present an opposite end of these models such that infragravity waves generate only horizontal forces (not vertical forces) on the seafloor to excite background Love and Rayleigh waves simultaneously. Although the atmospheric disturbance producing ultimately infragravity waves may play a part in generating directly the "hum," we will not discuss this possibility. The model is not precise at quantitative points and not intended to explain all of the features of Earth's hum.

[1]Institute for Research on Earth Evolution, Japan Agency for Marine-Earth Science and Technology, Yokosuka, Japan.
[2]Earthquake Research Institute, University of Tokyo, Tokyo, Japan.
[3]Institute of Space and Astronomical Science, Japan Aerospace Exploration Agency, Sagamihara, Japan.

0148-0227/10/2009JB006678

2. Observations

[3] In section 2 we summarize the recent observations that have to be taken into account for modeling the excitation source.

2.1. Source Locations

[4] *Rhie and Romanowicz* [2004] analyzed 2 year records of two networks in Japan and California to show that back-

ground Rayleigh waves at periods around 240 s have their origins mainly in the northern Pacific Ocean during Northern Hemisphere winter and in the Southern oceans during Southern Hemisphere winter in good correlation with the seasonal variation of the amplitudes of ocean waves. *Rhie and Romanowicz* [2006] made a more detailed analysis for two large "hum" events in Northern Hemisphere winter to locate their origins nearshore in California and northern Pacific. They inferred that generation of hum events comprises three elements: (1) generation of infragravity waves by nonlinear interaction of short-period ocean waves that occurs upon approach of a storm to the coast; (2) generation of long-period Rayleigh wave by interaction of infragravity waves with the seafloor; and (3) radiation of part of infragravity waves as free waves out into deep ocean to propagate over long distances to couple with the seafloor at distant coasts. *Kurrle and Widmer-Schnidrig* [2008] analyzed intensely 1 year records of seismic networks in Germany and California, supplemented with 8 year records, to show that large "hum" events are generated when the center of storms hits the Atlantic coastlines, suggesting that the interaction of ocean waves with shallow coastal regions is crucial for the coupling between ocean waves and seismic waves. Most recently *Bromirski and Gerstoft* [2009] analyzed 8 month records of the USArray to indicate that the primary and secondary source regions for the "hum" evens detected by the array are the Pacific coast of North America and the western coast of Europe, respectively. They demonstrated a good correlation between the hum events, ocean swell along coasts and infragravity waves to argue that large hum events are generated by infragravity waves in particular coastal regions. All of the above studies have indicated the generation of large hum events by interaction of infragravity waves with the seafloor in coastal regions. This does not imply, however, that the stationary hum activity has its origin only in coastal regions. *Nishida and Fukao* [2007] used the 13 year records of the IRIS global network stations to determine the 2-month-averaged source distribution of Earth's "hum" in spherical harmonics. They showed that the sources are located in the northern Pacific Ocean in Northern Hemisphere winter and in the southern hemispheric oceans in summer in agreement with the result of *Rhie and Romanowicz* [2004]. They showed that regardless of the seasons the source distribution is most dominated by the degree-0 component of spherical harmonics and secondarily by the degree-2 component with a power ratio of 10 to 1. They pointed out that if the sources are concentrated in shallow seas at depths less than 500 m, the relevant power ratio should be 10 to more than 4. Clearly, the observed ratio of 10 to 1 cannot be explained by a concentration of excitation sources only in shallow, coastal seas. The excitation sources must not be restricted to coastal regions but extend over much wider oceanic regions. This point is further substantiated by *Nishida et al.* [2008], who analyzed 1 year records of more than 600 Hi-Net tiltmeter stations in Japan to demonstrate that background Love and Rayleigh waves are strongest in directions from the ocean-continent borders, next strongest in directions from the deep ocean and weakest from the continent. The energy of waves from the ocean-continent borders is important because of the large amplitudes and the energy of waves from the deep ocean is significant as well because of the large source areas.

2.2. Love Wave Excitation

[5] The recent surprise in this field is the discovery of background toroidal oscillations in a frequency range from 3 to 7 mHz [*Kurrle and Widmer-Schnidrig*, 2008] or background Love waves in a range 10 to 30 mHz [*Nishida et al.*, 2008]. The observed amplitudes of the toroidal oscillations at several quietest sites in the world are comparable to those of the horizontal component of the spheroidal oscillations. The observed Love and Rayleigh waves traveling over the Japanese islands show mutually similar seasonal variations. Wave amplitudes depend strongly on whether waves are incident from the ocean-continent border or from the deep ocean floor or from the continent but the Love to Rayleigh amplitude ratio depends little on such incident directions [*Nishida et al.*, 2008]. We note that although seafloor topography in the ocean-continent borders is extremely anisotropic, the observed Love to Rayleigh wave amplitude ratio is similar to the one observed for the deep ocean where the bottom topography is largely isotropic. These observations suggest that background Love and Rayleigh waves are in large part generated at seafloors and radiated away more or less isotropically by the same mechanism(s) other than vertical pressure load acting on the seafloor. We propose a mechanism involving a linear interaction of infragravity waves with seafloor topography. The mechanism should work conceptually on seafloors at any depths but we focus our interest on deep seafloors where we can ignore the phase velocity and amplitude changes associated with propagation of infragravity waves across the topography, making the analysis extremely simple as developed below.

3. Tangential Force Generated by Topography-Coupled Infragravity Wave

[6] Our interest in this paper is background Love and Rayleigh waves in a frequency range from 5 to 20 mHz generated by infragravity waves in the same frequency range through a linear coupling process with the seafloor topography. Wavelengths of infragravity waves in this frequency range are on the order of 10 to 40 km in the deep ocean. We seek for the seafloor topography with the wavelengths of this order. According to *Menard* [1964, section 2.3], the most widespread physiographic forms on the face of Earth are the abyssal hills which cover 80 to 85% of the Pacific floor. Individual hills range in size up to a lateral extent of some 40 km and a height of some 300 or 400 m. Thus, infragravity waves in the deep ocean are expected to interact efficiently with these abyssal hills. Note that abyssal hills are at most 300–400 m high, an order of magnitude smaller than water depth of the deep ocean. Their slopes are also small, on the order of 0.01. The topography-related phase velocity change and the associated amplitude change of infragravity wave can be neglected, accordingly.

[7] Following *Lighthill* [1978], we consider horizontal propagation of infragravity wave. We take the z axis to be positive upward with the undisturbed sea surface at $z = 0$ and the undisturbed seafloor at $z = -h$. A velocity potential that represents a sinusoidal wave propagating in the positive x direction with wave number k is

$$\phi = \Phi_o \cosh[k(z+h)] \cos(\omega t - kx). \tag{1}$$

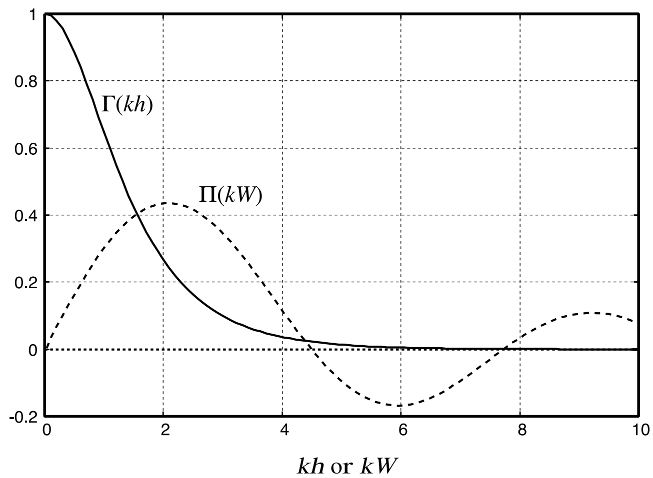

Figure 1. Hydrodynamic effect Γ as a function of kh and topographic coupling effect Π as a function of kW. Here k is the wave number of infragravity wave, h is water depth, and W is the half width of model abyssal hill.

The phase and group velocities c_o and U_o are given by

$$c_o = \frac{\omega}{k} = \sqrt{\frac{g}{k}\tanh kh}, \qquad U_o = \frac{d\omega}{dk} = \frac{c_o}{2}\left(1 + \frac{2kh}{\sinh 2kh}\right). \tag{2}$$

In the long-wave approximation ($kh \ll 1$), $c_o \approx U_o \approx \sqrt{gh}$. The excess pressure is

$$p_e = -\rho\frac{\partial\phi}{\partial t} = \rho\omega\Phi_o\cosh[k(z+h)]\sin(\omega t - kx) \tag{3}$$

the amplitude of which should be $\rho g\xi_o$ at $z = 0$, where ξ_o is the displacement amplitude of the sea surface disturbance and ρ is the density. Hence,

$$\Phi_o = \frac{g\xi_o}{\omega\cosh kh}. \tag{4}$$

We now disturb the seafloor as

$$z = -h + a_t(x, y). \tag{5}$$

We retain a linear problem by assuming that both $a_t(x, y)/h$ and bed slopes $\partial a_t/\partial x$, $\partial a_t/\partial y$ are small. In the presence of the bottom disturbance, the excess pressure p_e acting on a tilted bottom with angle β generates shear stress $\sigma_t \approx p_e \tan\beta$ and normal stress $\sigma_n \approx p_e$ on the undisturbed bottom horizon. Accordingly,

$$\sigma_t = [p_e]_{z=-h}\frac{\partial a_t}{\partial x}, \qquad \sigma_n = [p_e]_{z=-h} \tag{6}$$

where $|\partial a_t/\partial x| \ll 1$. We consider a circular cone hill with height H and bottom radius W, for which the impact of infragravity wave is independent of its incident azimuth.

$$\begin{aligned} a_t(x,y) &= a_t(r\cos\theta, r\sin\theta) \\ &= H(1 - r/W) \qquad r \le W \\ &= 0 \qquad r > W. \end{aligned} \tag{7}$$

The slope in the x direction is given by

$$\begin{aligned} \frac{\partial a_t}{\partial x} &= -\frac{H}{W}\cos\theta \qquad r \le W \\ &= 0 \qquad r > W \end{aligned}$$

so that the horizontal tangential stress generated by infragravity wave propagating in the x direction is

$$\begin{aligned} \sigma_t(r,\theta) &= -\frac{\rho\xi_o g}{\cosh(kh)}\frac{H}{W}\cos\theta\sin(\omega t - kr\cos\theta) \qquad r \le W \\ &= 0 \qquad r > W. \end{aligned} \tag{8}$$

The total tangential force acting on the seafloor is then given by

$$\begin{aligned} f_t &= \int_0^\infty\int_0^\infty \sigma_t(x,y)dxdy = \int_0^{2\pi} d\theta\int_0^W \sigma_t(r,\theta)rdr \\ &= \frac{\rho\xi_o g\cdot 4HW}{\cosh(kh)}\cos\omega t\cdot\int_0^{\pi/2}\eta(kW,\theta)d\theta \qquad \text{where} \end{aligned} \tag{9}$$

$$\eta(kW,\theta) = \frac{1}{kW}\left[-\cos(kW\cos\theta) + \frac{\sin(kW\cos\theta)}{kW\cos\theta}\right]. \tag{10}$$

Function $|\eta(kW, \theta)|$ in a range $0 \le \theta \le \pi/2$ takes its maximum at $\theta = 0$, decreases with increasing θ and becomes zero at $\theta = \pi/2$. We may roughly evaluate $\int_0^{\pi/2}\eta(kW, \theta)d\theta$ by replacing $\eta(kW, \theta)$ with $\eta(kW, 0)$ and truncating integration at $\theta = \pi/4$ (half of the whole integral range). Such a crude approximation leads to

$$f_t = \rho\xi_o g\cdot\pi HW\cdot\Gamma(kh)\Pi(kW)\cos\omega t \tag{11}$$

where Γ represents the hydrodynamic filtering effect:

$$\Gamma(kh) = \frac{1}{\cosh(kh)} \tag{12}$$

($0 < \Gamma \le 1$) and Π indicates the topographic coupling effect:

$$\Pi(kW) = \frac{\sin(kW) - kW\cos(kW)}{(kW)^2} \tag{13}$$

($0 < \Pi < 1$). Expression (11) can also be obtained by considering a pyramid circumscribing the circular cone with a common apex with height H. The bottom sides of the pyramid with length $2W$ are either parallel to or perpendicular to the wave-incident direction. For this hill geometry, the total tangential force can be derived rigorously as $f_t(pyramid) = \rho\xi_o g \cdot 4HW \cdot \Gamma(kh)\Pi(kW)\cos\omega t$. By correcting this expression for the difference in bottom area between the circular cone and its circumscribing pyramid, we obtain expression (11). Figure 1 shows Γ as a function of kh and Π as a function of kW. For a given water depth h, infragravity wave effectively senses the sea bottom if $kh < 1$. For a given bottom radius W, topographic coupling occurs efficiently for infragravity waves with wave numbers in a range $k_o - \Delta k/2 < k < k_o + \Delta k/2$ where

$$k_o \approx 2\pi/3W, \qquad \Delta k \approx \pi/3W. \tag{14}$$

This wave number range corresponds to the angular frequency range $\omega_o - \Delta\omega/2 < \omega < \omega_o + \Delta\omega/2$ where

$$\omega_o = c_o k_o$$
$$\Delta\omega = U_o \Delta k. \tag{15}$$

Here, phase and group velocities c_o and U_o are related to k_o through the dispersion relation (2). If the wave number is in a range (14), the horizontal component of the excess pressure acting on one side of the hillslope and that on the opposite side are mutually in phase so that they together generate horizontal force effectively. If the wave number is well below this range, the horizontal components on the two sides are almost completely out of phase so that they together cancel out and generate horizontal force poorly. If the wave number is well above the range (14), on one hand, the excess pressure is rapidly sinusoidal on either side of the hillslope so that little net horizontal force is produced. Only in the wave number range (14), coupling can occur efficiently. We should note that this topographic coupling mechanism generates only horizontal force but not vertical force because the total normal force f_n acting on the seafloor is given by

$$f_n = \int_{-\infty}^{\infty}\int_{-\infty}^{\infty} \sigma_n dxdy \approx \int_{-\infty}^{\infty}\int_{-\infty}^{\infty} [p_e]_{z=-h} dxdy = 0. \tag{16}$$

The expression of normal stress σ_n correct to the first order of H/W contains no term contributing to the net force vertically acting on the seafloor.

[8] The hills topography can be modeled to a reasonable degree as a random distribution of independent hills [*Bell*, 1975]. Each of the randomly distributed hills is passed by infragravity waves from many directions. We assume that infragravity waves incident from different directions are mutually uncorrelated. The power spectral density (PSD) of the resultant temporal surface pressure fluctuation is denoted by $S^{press}(f)$. Following (11), the PSD of the tangential force generated at a hill is given by:

$$S^{force}(f, W) = S^{press}(f) \cdot H^2[\pi W \Gamma(kh)\Pi(kW)]^2 \tag{17}$$

where $f = \omega/2\pi$, k is the wave number as a function of frequency f and water depth h. There is an empirical relation between H^2 and W:

$$H^2 \approx BW \tag{18}$$

(see Appendix A). A one-dimensional version of our seafloor topography model is a random distribution of triangle hills, for which the number of hills with half widths greater than W is given by

$$N_1(W) = \frac{n_o}{W} \tag{19}$$

per unit length (see Appendix A). The nondimensional number n_o may be determined from the statistics of abyssal hills topography. The fractal dimension associated with the distribution (19) is 1 in coincidence with the Euclidian dimension. This coincidence implies that the fractal dimension associated with the random distribution of circular-cone hills is 2 so that the number of hills with radii greater than W is given by

$$N_2(W) = \frac{4}{\pi}\left(\frac{n_o}{W}\right)^2 \tag{20}$$

per unit area, where $4/\pi$ is a geometric factor that corrects for the areal difference between a circle with radius W and a square with half-length W. Although the spatial correlation of infragravity waves is characterized by a long, oscillatory tail [*Webb*, 1986], the tangential forces generated at different hills are mutually uncorrelated because of the spatially random nature of hills distribution. The resultant tangential force PSD per unit area is then given by

$$\begin{aligned} T(f) &= \int_0^\infty S^{force}(f, W) \cdot \left(-\frac{dN_2}{dW}\right) dW \\ &\approx S^{press}(f) \cdot 8\pi n_o^2 B \frac{\Gamma^2(kh)}{k} \int_0^\infty \Pi^2(x)dx \\ &\approx S^{press}(f) \cdot 13 n_o^2 Bh \frac{\Gamma^2(kh)}{kh} \end{aligned} \tag{21}$$

where wave number k is related to frequency $f = \omega/2\pi$ through the dispersion relation of infragravity wave (2). The integrand with respect to x takes its maximum at $x = x_o \approx 2.08$ and converges monotonically to zero as $x \to 0$ and $x \to \infty$. Although expression (20) for $N_2(W)$ is not valid for very small W and for very large W, contributions from such ranges to the integration are negligibly small for any form of N_2 function so that we may safely set the lower and upper bounds of the integration at zero and infinity, respectively. Following the discussion developed in Appendix A, we use the values of $n_o = 0.072$ and $B = 11$ m. Figure 2 shows $T(f)$ as a function of f for typical ocean depths of 6000, 4500, 3000 and 1500 m with a representative value of 10^4 Pa^2/Hz for $S^{press}(f)$ in the deep ocean [*Webb et al.*, 1991; *Uchiyama and McWilliams*, 2008]. The tangential force PSD $T(f)$ decreases monotonically as frequency increases. Above ~5 mHz, the decrease is more rapid for the deeper ocean. This tendency is reversed below ~5 mHz, where equation (21) reduces to:

$$T(f) \to S^{press}(f) \cdot 13 n_o^2 \frac{B}{\omega}\sqrt{gh}$$

as $kh \to 0$ so that the tangential force PSD $T(f)$ decreases as $\sqrt{h}$ with decreasing water depth h.

4. Excitation of Seismic Surface Waves

[9] The wavelengths of seismic surface waves are more than an order of magnitude larger than the widths of abyssal hills. Accordingly, the tangential force generated at a hill can be approximated as a point force to excite seismic surface waves. Our formulation of seismic excitation is made in the cylindrical coordinates (r, ϕ, z) with the z axis vertically downward (sea surface at $z = 0$, sea bottom at $z = h$), where a horizontal point force of the form $F_t(\omega)e^{i\omega t}$ is applied at $r = 0$ and $z = h$ in a radial direction with azimuth ψ from the

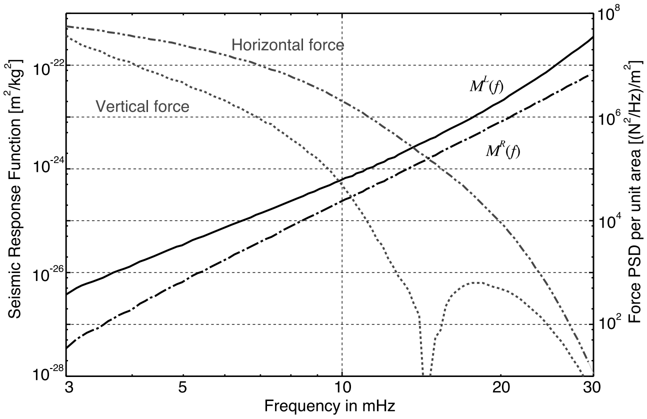

Figure 2. Medium response term $M^L(f)$ for Love waves and $M^R(f)$ for Rayleigh waves (scale is shown on the left axis). The horizontal force term $T(f)$ for the composite model ocean and the vertical force term $V(f)$ required to keep the Love to Rayleigh wave energy ratio constant ($R' = 1.3$) are also shown (scale is shown on the right axis).

x axis. The resultant horizontal displacement of the fundamental Love mode at (r, ϕ, z) is expressed as

$$\vec{u}^L = \frac{F_t(\omega)\sin(\psi-\phi)\cdot y_1^L(h)y_1^L(z)}{8c^LU^LI_1^L}\vec{\phi}\sqrt{\frac{2}{\pi k^L r}} \cdot \exp\left[i\left(\omega t - k^L r - \frac{\pi}{4}\right)\right] \tag{22}$$

where angular frequency ω is related to seismic wave number k^L, phase velocity c^L and group velocity U^L through the surface wave dispersion relation, $y_1^L(z)$ is a Love mode eigenfunction and

$$I_1^L = \frac{1}{2}\int_0^\infty \rho\left[y_1^L\right]^2 dz$$

where ρ is density as a function of z [*Aki and Richards*, 1980]. The horizontal displacement of the fundamental Rayleigh mode at (r, ϕ, z) is expressed as

$$\vec{u}^R = \frac{F_t(\omega)\cos(\psi-\phi)\cdot y_3^R(h)y_3^R(z)}{8c^RU^RI_1^R}\vec{r}\sqrt{\frac{2}{\pi k^R r}} \cdot \exp\left[i\left(\omega t - k^R r - \frac{\pi}{4}\right)\right] \tag{23}$$

where

$$I_1^R = \frac{1}{2}\int_0^\infty \rho\left\{\left[y_1^R\right]^2 + \left[y_3^R\right]^2\right\}dz.$$

Here $y_1^R(z)$, $y_3^R(z)$ are two Rayleigh mode eigenfunctions [*Aki and Richards*, 1980]. In (22) and (23) the effect of attenuation may be included by multiplying a diminution factor $\exp(-\alpha r)$ where seismic attenuation coefficient α is related to quality factor Q as

$$\alpha = \frac{k}{2Q} \tag{24}$$

and the parameters involved are understood as Q^L, α^L, k^L for Love waves and Q^R, α^R, k^R for Rayleigh waves.

[10] In our model the horizontal point forces uniformly distribute at random in space and orientation. The magnitudes of these distributed forces are defined by their PSDs per unit area, $T(f)$. The orientations of these forces ψ (measured from the x axis) are azimuthally at random. We evaluate the impact of these distributed forces at the origin (r = 0) of a semicircular ocean with uniform water depth h developed on the positive side of the x axis within a radius of $r = r_o$. By referring to (22), the acceleration PSD of Love wave at depth z is expressed as $S^L(f) = T(f)M^L(f)$ where

$$\begin{aligned} M^L(f) &= \omega^4\left[\frac{y_1(h)y_1(z)}{8c^LU^LI_1^L}\right]^2\int_0^\pi d\varphi\int_0^{2\pi}d\psi\int_0^{r_o} \\ &\quad \cdot\sin^2(\psi-\phi)\frac{2}{\pi k^L r}\exp\left(-2\alpha^L r\right)rdr \\ &= 2\pi\omega^2\left[\frac{y_1^L(h)y_1^L(z)}{8U^LI_1^L}\right]^2 Q^L\left[1-\exp\left(-k^Lr_o/Q^L\right)\right]. \end{aligned} \tag{25}$$

Here $\varphi = \pi - \phi$ is the azimuth to a force point on the seafloor from the observation point at the coast located at the origin of the semicircular ocean. The medium response $M^L(f)$ is calculated at depth $z = h$ using the Earth model PREM [*Dziewonski and Anderson*, 1981] which has a 3 km thick model ocean. By referring to (23), we obtain the expression for the acceleration PSD of horizontal Rayleigh wave as $S^R(f) = T(f)M^R(f)$ where

$$\begin{aligned} M^R(f) &= \omega^4\left[\frac{y_3^R(h)y_3^R(z)}{8c^RU^RI_1^R}\right]^2\int_0^\pi d\varphi\int_0^{2\pi}d\psi\int_0^{r_o} \\ &\quad \cdot\cos^2(\psi-\phi)\frac{2}{\pi k^R r}\exp\left(-2\alpha^R r\right)rdr \\ &= 2\pi\omega^2\left[\frac{y_3^R(h)y_3^R(z)}{8U^RI_1^R}\right]^2 Q^R\left[1-\exp\left(-k^Rr_o/Q^R\right)\right]. \end{aligned} \tag{26}$$

The kinetic energy ratio of Love to Rayleigh wave is given by

$$R = \frac{M^L(f)I_1^L}{\left[y_1^L(z)\right]^2}\bigg/\frac{M^R(f)I_1^R}{\left[y_3^R(z)\right]^2} \tag{27}$$

which does not depend on any detail of the source term. In our traveling wave approach, continents have been treated simply as regions having no excitation sources. A similar but more elaborated treatment was made in the normal mode approach of *Nishida and Fukao* [2007]. *Webb* [2007, 2008], on the other hand, evaluated the intensity of sources on continental shelves by assuming a uniform, random distribution of excitation sources over the whole surface of the attenuating spherical Earth and treated continents as regions across which extra attenuation occurs as traveling waves. Such a mixed treatment of normal-mode approach and traveling-wave approach would require a theoretical justification. Figure 2 shows the medium response $M^L(f)$ for Love wave and $M^R(f)$ for Rayleigh wave where a representative value of 5000 km is used for the radius r_o of the semicircular ocean. Both the Love and Rayleigh wave responses increase monotonically with increasing frequency.

[11] We now make an order of estimate of the acceleration PSDs $S^L(f)$ and $S^R(f)$, using (21) and (25) for Love waves and using (21) and (26) for Rayleigh waves. We take the

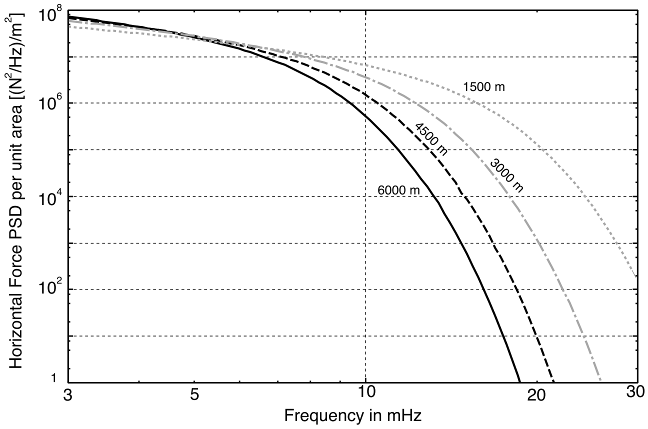

Figure 3. Tangential force power spectral density (PSD) per unit area $T(f)$ for several water depths in a frequency range 3–30 mHz.

radius of the semicircular ocean to be r_o = 5000 km, which gives an area approximately equal to the area of the hum source region in Northern Hemisphere winter as estimated by *Nishida and Fukao* [2007] using the global seismic network data. For this model ocean, the source term $T(f)$ is calculated as a weighted average of those for the four depths 6000, 4500, 3000 and 1500 m (Figure 3). The assigned weights are 13, 47, 23, and 7% corresponding to the areal proportions of the ocean depth ranges 6000 ± 750, 4500 ± 750, 3000 ± 750, and 1500 ± 750 m, respectively. Contribution from the deeper ocean is neglected because of the minor areal proportion. Contribution from the ocean shallower than 750 m depth (10% of the whole ocean surface) is not considered, not because topographic coupling is unimportant at such shallow depths but because it cannot be handled by the present simple theory. Figure 2 shows the source term $T(f)$ for our model ocean, and Figure 4 shows the power spectra of horizontal ground acceleration for Love and Rayleigh waves calculated with this $T(f)$. The maximum PSD of Love wave at 8.3 mHz is about three times as large as the maximum PSD of Rayleigh wave at 9.3 mHz. Figure 5 shows the kinetic energy ratio R of Love to Rayleigh wave as a function of frequency calculated by (27). In the frequency range of our interest (5–20 mHz), the R curve forms a broad trough with values around 1.3. The R value remains to be less than 1.8 in the whole frequency range of our interest, outside of which the value increases rapidly.

5. Comparison With the Observations

[12] In section 5 we compare our model with the observations, although a quantitative discussion is limited by large uncertainties associated with our statistical treatment of seafloor topography and our gross approximation for source area configuration. Our major interest is a semiquantitative comparison of the spectral behaviors between the observations and the model in a frequency range 5–20 mHz. Figure 4 shows the model acceleration PSD curves for Love and Rayleigh waves in comparison with the PSD values obtained by *Nishida et al.* [2008] at frequencies above 10 mHz. The model PSD curves of Love and Rayleigh waves agree with the observed PSD values within a factor of a few in a frequency range between 10 and 20 mHz. The observed trends are different from the model trends, however.

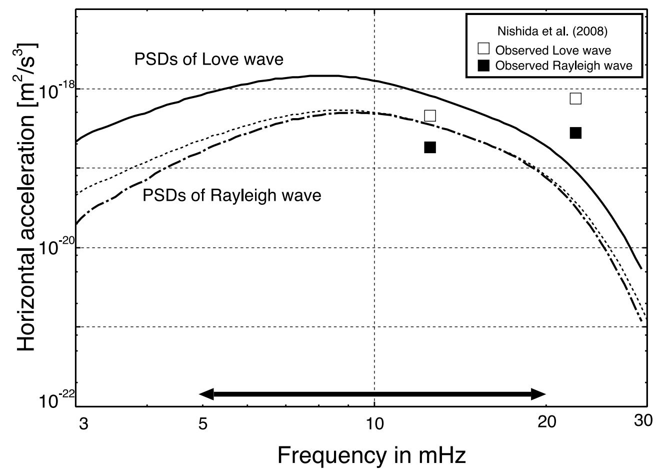

Figure 4. Horizontal acceleration PSDs of Love and Rayleigh waves in a frequency range of 3–30 mHz for our model ocean. The wave height PSD of infragravity wave is assumed to be frequency independent. The impact of the addition of the vertical force term $V(f)$ to the horizontal force term $T(f)$ is shown by the dotted curve. The observed PSDs of horizontal Love and Rayleigh waves above 10 mHz [*Nishida et al.*, 2008] are also shown. The frequency range of our interest, 5–20 mHz, is indicated by the arrow.

[13] The Love to Rayleigh wave amplitude ratio or kinetic energy ratio is an important measure to evaluate our model. Figure 5 shows the model kinetic energy ratio between 3 and 30 mHz, which is compared with the recent two observations. According to *Nishida et al.* [2008], the observed energy ratio is almost constant, ~1.25, above 10 mHz up to 50 mHz. The

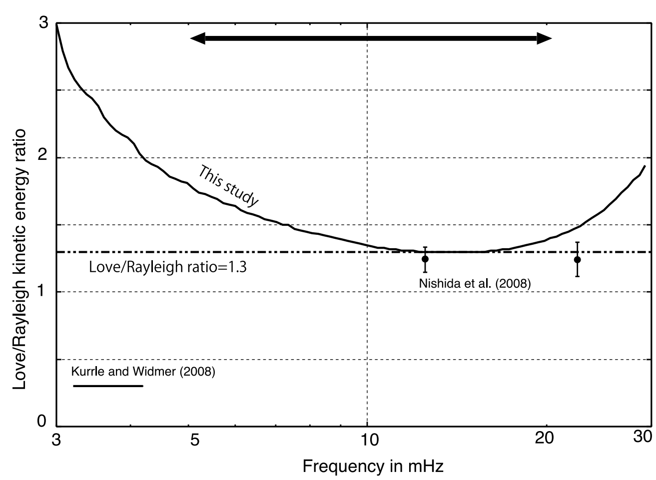

Figure 5. Kinetic energy ratio of Love to Rayleigh waves in a frequency range of 3–30 mHz. The observed energy ratio above 10 mHz [*Nishida et al.*, 2008] and that at frequencies around 4 mHz [*Kurrle and Widmer-Schnidrig*, 2008] are also shown. The constant ratio line (R' = 1.3) is drawn to discuss the gap between the present model and the observation by *Nishida et al.* [2008]. The frequency range of our interest, 5–20 mHz, is indicated by the arrow.

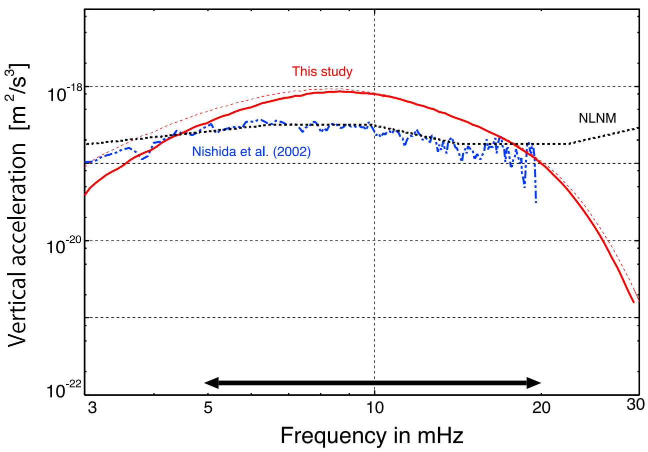

Figure 6. Model vertical acceleration PSD of Rayleigh waves in frequency range 3–30 mHz. Impact of addition of the vertical force term $V(f)$ to the horizontal force term $T(f)$ is shown by the dotted curve. The observed vertical PSDs of the background spheroidal oscillations (Rayleigh waves) [*Nishida et al.*, 2002] and the New Low Noise Model (NLNM) of *Peterson* [1993] are also shown. The frequency range of our interest, 5–20 mHz, is indicated by the arrow.

kinetic energy ratio curve in our model shows a broad trough with values around 1.3 in good agreement with the observed ratio. This agreement is limited in a frequency range 10–16 mHz, however. Above ~20 mHz, the model ratio curves tend to increase with increasing frequency in contrast to the observed trend. *Kurrle and Widmer-Schnidrig* [2008] reported that the horizontal amplitudes of the toroidal and spheroidal modes are approximately the same in a frequency range of 3.2 to 4.2 mHz. In order to convert this observation into the kinetic energy ratio of toroidal to spheroidal modes, we set $M^L(f)/M^R(f) \approx 1$ in (27) to obtain an energy ratio of about 0.3. This value is also plotted in Figure 5. Clearly, the observed energy ratio is much lower than the model energy ratio.

[14] The spectral shape of the vertical component of background Rayleigh waves is well known in a wide frequency range, which can serve as a check of our model. Figure 6 shows the model power spectrum of vertical Rayleigh waves which is obtained by multiplying $[y_1^R(h)/y_3^R(h)]^2$ to the model power spectrum of horizontal Rayleigh waves. In Figure 6 we superpose the observed power spectrum of background Rayleigh waves (or spheroidal oscillations) of vertical component [*Nishida et al.*, 2002] and the New Low Noise Model (NLNM) of *Peterson* [1993]. Either the observed spectrum or the NLNM exhibits a plateau feature near 8 mHz, in agreement with the model spectrum, although the model plateau is more sharply peaked. The observed and model PSD values coincide with each other within a factor of a few in a frequency range 5–20 mHz. The NLNM changes the spectral trend around 20 mHz, above which it begins to increase with increasing frequency, suggesting that some different excitation mechanism becomes more dominant above ~20 mHz.

6. Discussion

[15] We have developed a model that can explain semi-quantitatively the simultaneous excitation of background torsional and spheroidal oscillations (or background Love and Rayleigh waves) as observed by *Kurrle and Widmer-Schnidrig* [2008] and *Nishida et al.* [2008]. The frequency range of our interest is 5–20 mHz. The acceleration power spectrum of Rayleigh waves for a model ocean shows a plateau feature near 8 mHz in agreement with the observed background Rayleigh wave spectrum [*Nishida et al.*, 2002] and with the New Low Noise Model (NLNM) of ground motion [*Peterson*, 1993], although the observed vertical Rayleigh wave spectrum (or NLNM) shows a broader plateau than the model spectrum. The observed (or NLMN) PSD and our model PSD are in agreement within a factor of a few in a frequency range 5–20 mHz. Above 20 mHz, the NLMN tends to sharply deviate from the model spectrum. The model kinetic energy ratio of Love to Rayleigh wave is ~1.3 in a frequency range 10–16 mHz, which can be well compared to the observed energy ratio of 1.25 [*Nishida et al.*, 2008], while the discrepancy increases outside on both the positive and negative sides, where preferential generation of Rayleigh waves by action of vertical forces may be required. In order to obtain some idea of the relative importance of vertical forces to horizontal forces, we add a random distribution of vertical forces to the random distribution of horizontal forces so that the energy ratio is kept constant at 1.3 over the whole frequency range. Let the required PSD of the vertical forces per unit area be $V(f)$. Because the medium response to the vertical force distribution is expressed as $M^R[y_1^R(h)/y_3^R(h)]^2$ for horizontal Rayleigh wave and $M^R[y_1^R(h)/y_3^R(h)]^4$ for vertical Rayleigh wave, the kinetic energy ratio of Love to Rayleigh wave in the coexisting case of $T(f)$ and $V(f)$ is given by

$$R' = \frac{R}{1 + [V(f)/T(f)]\left[y_1^R(h)/y_3^R(h)\right]^2}$$

where R is defined in (27). We search for $V(f)$ with which $R' = 1.3$ uniformly over the whole frequency range. The vertical force PSD $V(f)$ so obtained is compared to the horizontal force PSD $T(f)$ in Figure 2. The deep trough of $V(f)$ at 10–16 mHz indicates that it is unnecessary to introduce vertical forces in this frequency range to explain the observed Love to Rayleigh wave energy ratio.

[16] We calculate the horizontal and vertical acceleration PSDs of Rayleigh waves for the vertical force term $V(f)$, which are then added to those for the horizontal force term $T(f)$. The resultant horizontal and vertical spectra are compared with the original spectra calculated for $T(f)$ (Figures 4 and 6). Figure 6 indicates that addition of vertical forces tends to better explain the observed hum amplitudes at frequencies below 5 mHz. At frequencies above 20 mHz, however, addition of vertical forces contributes little to closing a gap between the observed (NLNM) curve and the model curve. This indicates that above 20 mHz some mechanism(s) that can generate both horizontal and vertical forces has to be invoked. We here suggest shallow-seas topographic coupling as one of such mechanisms.

[17] In our topographic coupling model the contribution from shallow seas at depths less than 750 m depth (in large part less than 250 m) has not been taken into account. In such shallow (largely coastal) seas, infragravity wave across the topography changes its phase velocity and amplitude and neither of these effects can be handled in our simple

theory. The amplitude change of infragravity wave across the topography should produce a net normal force on the seafloor upon coupling of the wave with topography. Topographic coupling occurring in shallow seas is unique in that it produces not only tangential force but also normal force on the seafloor. The tangential force generates Love and Rayleigh waves with an energy ratio given by (27), while the normal force generates Rayleigh waves preferentially. The shallow seas contribution is expected to be important particularly in the higher-frequency range, where the effect of hydrodynamic filtering degrades contributions from deeper, wider oceans (see Figure 3). Taking this possible shallow seas contribution and the various uncertainties in model parameters into account, our model in a frequency range from 5 well up to 20 mHz is reasonably consistent with the observations of the Rayleigh wave spectral plateau around 8 mHz, the PSD levels of Love and Rayleigh waves, and the Love to Rayleigh wave kinetic energy ratio as well as its azimuthally isotropic nature. At frequencies below 5 mHz, the observed PSD of spheroidal oscillations [*Nishida et al.*, 2002] tends to be greater than the model PSD (Figure 6) and the observed kinetic energy ratio of toroidal to spheroidal oscillations [*Kurrle and Widmer-Schnidrig*, 2008] becomes significantly lower than the corresponding model ratio (Figure 5). These deviations imply that below ~5 mHz some mechanism(s) of exciting Rayleigh waves preferentially should act in addition to the topographic coupling mechanism. The suggested mechanisms include the nonlinear interaction of infragravity waves acting as pressure forces on the seafloor of continental shelf [*Tanimoto*, 2005, 2007; *Webb*, 2007, 2008] and the atmospheric disturbance loading on the sea surface that would give a straightforward explanation for the observed resonant oscillations between the solid Earth and the atmosphere [*Nishida et al.*, 2000]. At frequencies above 20 mHz, we have suggested that topographic coupling in shallow seas plays a role. This shallow process might be somehow related to the microseisms activity at the primary frequencies between 50 and 100 mHz, which is known to be strongly correlated with the activities of oceanic swells [*Okeke and Asor*, 2000; *Stehly et al.*, 2006]. The suggested mechanisms in this frequency range include propagation of oceanic swells along the coastal slope that produces the vertical pressure force to emit Rayleigh waves in all the directions [*Darbyshire and Okeke*, 1969] and the horizontal frictional force to emit Love waves in the direction parallel to the coastal line [*Friedrich et al.*, 1998].

7. Conclusions

[18] In the Pacific, about 90% of the seafloor is occupied by hills with heights 100 to 300 m and slopes of the order of 0.01 [*Pelinovsky*, 2007]. Such hills with sizes up to some 40 km are of our major interest because their coupling with infragravity waves can generate background torsional and spheroidal oscillations as observed by *Kurrle and Widmer-Schnidrig* [2008] or background Love and Rayleigh waves as observed by *Nishida et al.* [2008]. Coupling occurs when the predominant wavelengths of infragravity waves and seafloor topography match each other. The most important feature of this coupling is to generate horizontal tangential stress on the seafloor to the first order of the hillslope but to generate vertical normal stress only to the second order. Such tangential stress can excite by its nature Love and Rayleigh waves simultaneously. Although the radiation patterns of Love and Rayleigh waves from a single event of coupling are very different from each other, random propagation of infragravity waves across randomly distributed hills would make the radiation fields effectively uniform.

[19] The Love and Rayleigh wave acceleration PSDs can be expressed as the product of the source term and the medium response term. The medium response term describes seismic response to a uniform, random distribution of point horizontal forces of unit magnitudes on a given source area. The source term describes the intensity of this force distribution per unit source area. We have evaluated the source intensity by taking a weighted average of the contributions from oceans at various depths. Low-frequency seismic surface waves have their excitation sources all the way from shallow to deep oceans with decreasing source intensity with decreasing ocean depth. However, the excitation sources for higher-frequency seismic surface waves are limited to shallower oceans. The model Rayleigh wave spectrum in a range 5 to 20 mHz is in fair agreement with the observed background Rayleigh wave spectrum [*Nishida et al.*, 2002] and the NLNM spectrum [*Peterson*, 1993]. The model kinetic energy ratio curve of Love to Rayleigh wave has a broad trough at 10–16 mHz where the energy ratio is ~1.3 in agreement the observed value of 1.25 above 10 mHz [*Nishida et al.*, 2008]. The model energy ratio rapidly increases with decreasing frequency below 5 mHz and with increasing frequency above 20 mHz in poor agreement with the observations of background toroidal and spheroidal oscillations by *Kurrle and Widmer-Schnidrig* [2008] and those of background Love and Rayleigh waves by *Nishida et al.* [2008]. Below 5 mHz, some mechanism(s) of exciting Rayleigh waves preferentially must act in addition to the topographic coupling mechanism. Contribution of topographic coupling in shallow seas is not taken into account in our simple model but should be important especially at frequencies above ~20 mHz, in part because infragravity waves are largely generated and trapped in shallow seas [e.g., *Webb*, 2007] and in part because their coupling with topography generates not only tangential force but also normal force on the seafloor.

Appendix A: Hills Topography

[20] The statistical nature of seafloor topography has been discussed [*Bell,* 1975, 1979; *Malinverno,* 1995; *Goff et al.,* 2004]. Despite the recent progress in high-resolution mapping technique, our knowledge of fine structure of seafloor topography still relies on a limited number of detailed survey profiles. The results obtained from such surveys may not always be applied to other areas. Bearing this lack of comprehensiveness in mind, we use the classic results of *Bell* [1975, 1979] mainly because of ease of implementing them into our model. According to *Bell* [1975], the hills topography can be modeled to a reasonable degree as a random distribution of independent hills. The power spectrum of hills topography in one dimension decays as the inverse square of wave number above the effective low wave number cutoff at about 0.025 cycles/km which corresponds to an upper limit of about 40 km on the size of the hills. Although the power spectrum of abyssal hills topography tends to flatten out at the lower wave numbers, such a

flattening characteristic is hidden in the composite spectrum including the midoceanic ridges and other features considered to be deterministic on the scale of abyssal hills [*Bell*, 1975]. This composite spectrum shows a coherent continuation of spectral decay as the inverse square of wave number even below 0.025 cycles/km. The one-dimensional seafloor roughness in a scale from 0.1 to 100 km is then characterized by the power spectrum:

$$G(k) = \frac{C}{k^2} \tag{A1}$$

with $C \approx 2.2$ m [*Bell*, 1979]. Wave number k is related to wavelength λ as $k = 2\pi/\lambda$. Although the spectral form of (A1) is valid over several orders of wave number, we restrict our attention to a narrow range corresponding to hill sizes of 10–40 km, only where infragravity waves can couple the seafloor topography efficiently in the frequency range of our interest.

[21] We express the one-dimensional seafloor topography by a series of statistically independent hills that are distributed at random uniformly over the bottom. A hill is approximated by a triangle with height H and half-width W. The energy spectral density of this triangle function is given by

$$\psi(k, W) = H^2 W^2 \left[\frac{\sin(kW/2)}{kW/2}\right]^4. \tag{A2}$$

The PSD of seafloor topography is expressed as

$$G(k) = \int_0^\infty \psi(k, W)\left(-\frac{dN_1}{dW}\right) dW \tag{A3}$$

where $N_1(W)$ is the number of hills with half widths greater than W per unit length. *Bell* [1975] showed that $-dN_1/dW$ behaves empirically as W^{-2} if $W > W_c$ where $2W_c \approx 0.5$ km. In this range of W we write

$$-\frac{dN_1}{dW} = \frac{n_o}{W^2}. \tag{A4}$$

This expression is equivalent to (19) in the text. *Bell* [1975] also obtained such an empirical relation that

$$H_a^2 \approx AW_a \tag{A5}$$

where H_a and W_a are the maximum height of a hill and its half width along the survey route which may not always intersect the hill peak. On the basis of a scatterplot of height versus breadth of hills, *Bell* [1975] obtained an empirical value of $A \approx 4$ m. Assuming a three-dimensional hill geometry to be a circular cone with peak height H and bottom radius W, we evaluate the expected value of H_a^2 as an average of the squared height values along a profile that crosses the hill peak, namely, $H_a^2 = H^2/3$. We then evaluate the expected value of W_a as the half width of the profile along which the maximum height is $H/\sqrt{3}$. The squared peak height H^2 is then related to the bottom radius W as

$$H^2 = BW \tag{A6}$$

where

$$B \approx 2.72A \approx 10.9 \text{ m}. \tag{A7}$$

Insertion of (A2), (A4) and (A6) into (A3) yields the PSD of model seafloor topography:

$$\begin{aligned} G(k) &\approx n_o B \cdot \int_{0_c}^\infty W\left[\frac{\sin(kW/2)}{kW/2}\right]^4 dW \\ &= 4\frac{n_o B}{k^2} \cdot \int_0^\infty x\left[\frac{\sin(x)}{x}\right]^4 dx \\ &\approx 2.8\frac{n_o B}{k^2}. \end{aligned} \tag{A8}$$

In (A8) the integrand with respect to x takes its maximum at $x = x_o \approx 1.16$ and converges monotonically to zero as $x \to 0$ and $x \to \infty$. Although expression (A4) is not valid for very small W ($<W_c$) and for very large W ($\gg 1/k$), contributions to the integration from such ranges are negligibly small for any form of the hill geometry so that we may safely set the lower and upper bounds of the integration at zero and infinity, respectively. Comparison of (A8) with (A1) implies, using (A7), that $n_o \approx 0.072$.

[22] **Acknowledgments.** We thank Editor John Mutter, the Associate Editor, and the two anonymous referees for their constructive comments, which improved the original manuscript greatly.

References

Aki, K., and P. G. Richards (1980), *Quantitative Seismology, Theory and Methods*, 557 pp., W. H. Freeman, New York.
Bell, T. H. (1975), Statistical features of sea floor topography, *Deep Sea Res.*, *22*, 883–892.
Bell, T. H. (1979), Mesoscale sea floor roughness, *Deep Sea Res., Part A*, *26*, 65–76.
Bromirski, P. D., and P. Gerstoft (2009), Dominant source regions of the Earth's "hum" are coastal, *Geophys. Res. Lett.*, *36*, L13303, doi:10.1029/2009GL038903.
Darbyshire, J., and E. O. Okeke (1969), A study of primary and secondary microseisms recorded in Anglesey, *Geophys. J. Int.*, *17*, 63–92.
Dziewonski, A., and D. Anderson (1981), Preliminary reference earth model, *Phys. Earth Planet. Inter.*, *25*, 297–356, doi:10.1016/0031-9201(81)90046-7.
Ekström, G. (2001), Time domain analysis of Earth's long-period background seismic radiation, *J. Geophys. Res.*, *106*, 26,483–26,494, doi:10.1029/2000JB000086.
Friedrich, A., F. Krüger, and K. Klinge (1998), Ocean-generated microseismic noise located with the Gräfenberg array, *J. Seismol.*, *2*, 47–64, doi:10.1023/A:1009788904007.
Fukao, Y., K. Nishida, N. Suda, K. Nawa, and N. Kobayashi (2002), A theory of the Earth's background free oscillations, *J. Geophys. Res.*, *107*(B9), 2206, doi:10.1029/2001JB000153.
Goff, J. A., W. H. F. Smith, and K. M. Marks (2004), The contribution of abyssal hill morphology and noise to altimetric gravity fabric, *Oceanography*, *17*, 24–37.
Kobayashi, N., and K. Nishida (1998), Continuous excitation of planetary free oscillations by atmospheric disturbances, *Nature*, *395*, 357–360, doi:10.1038/26427.
Kurrle, D., and R. Widmer-Schnidrig (2008), The horizontal hum of the Earth: A global background of spheroidal and toroidal modes, *Geophys. Res. Lett.*, *35*, L06304, doi:10.1029/2007GL033125.
Lighthill, J. (1978), *Waves in Fluids*, 504 pp., Cambridge Univ. Press, New York.
Malinverno, A. (1995), Fractals and ocean floor topography: A review and a model, in *Fractals in the Earth Sciences*, edited by C. C. Barton and P. R. La Pointe, pp. 107–130, Springer, New York.
Menard, W. H. (1964), *Marine Geology of the Pacific*, 271 pp., McGraw-Hill, New York.

Nawa, K., N. Suda, Y. Fukao, T. Sato, Y. Aoyama, and K. Shibuya (1998), Incessant excitation of the Earth's free oscillations, *Earth Planets Space*, *50*, 3–8.

Nishida, K., and Y. Fukao (2007), Source distribution of Earth's background free oscillations, *J. Geophys. Res.*, *112*, B06306, doi:10.1029/2006JB004720.

Nishida, K., N. Kobayashi, and Y. Fukao (2000), Resonant oscillations between the solid earth and the atmosphere, *Science*, *287*, 2244–2246, doi:10.1126/science.287.5461.2244.

Nishida, K., N. Kobayashi, and Y. Fukao (2002), Origin of Earth's ground noise from 2 to 20 mHz, *Geophys. Res. Lett.*, *29*(10), 1413, doi:10.1029/2001GL013862.

Nishida, K., H. Kawakatsu, Y. Fukao, and K. Obara (2008), Background Love and Rayleigh waves simultaneously generated at the Pacific Ocean floors, *Geophys. Res. Lett.*, *35*, L16307, doi:10.1029/2008GL034753.

Okeke, E., and V. Asor (2000), On the microseisms associated with coastal sea waves, *Geophys. J. Int.*, *141*, 672–678, doi:10.1046/j.1365-246x.2000.00103.x.

Pelinovsky, E. (2007), Hydrodynamics of tsunami waves, in *Waves in Geophysical Fluids: Tsunamis, Rogue Waves, Internal Waves and Internal Tides*, edited by J. Grue and K. Trulsen, pp. 1–48, Springer, New York.

Peterson, J. (1993), Observations and modeling of seismic background noise, *U.S. Geol. Surv. Open File Rep.*, *93–322*, 1.

Rhie, J., and B. Romanowicz (2004), Excitation of Earth's continuous free oscillations by atmosphere-ocean-seafloor coupling, *Nature*, *431*, 552–556, doi:10.1038/nature02942.

Rhie, J., and B. Romanowicz (2006), A study of the relation between ocean storms and the Earth's hum, *Geochem. Geophys. Geosyst.*, *7*, Q10004, doi:10.1029/2006GC001274.

Stehly, L., M. Campillo, and N. M. Shapiro (2006), A study of the seismic noise from its long-range correlation properties, *J. Geophys. Res.*, *111*, B10306, doi:10.1029/2005JB004237.

Suda, N., K. Nawa, and Y. Fukao (1998), Earth's background free oscillations, *Science*, *279*, 2089–2091, doi:10.1126/science.279.5359.2089.

Tanimoto, T. (2001), Continuous free oscillations: Atmosphere–solid Earth coupling, *Annu. Rev. Earth Planet. Sci.*, *29*, 563–584, doi:10.1146/annurev.earth.29.1.563.

Tanimoto, T. (2005), The oceanic excitation hypothesis for the continuous oscillations of the Earth, *Geophys. J. Int.*, *160*, 276–288, doi:10.1111/j.1365-246X.2004.02484.x.

Tanimoto, T. (2007), Excitation of normal modes by non-linear interaction of ocean waves, *Geophys. J. Int.*, *168*, 571–582, doi:10.1111/j.1365-246X.2006.03240.x.

Tanimoto, T., J. Um, K. Nishida, and N. Kobayashi (1998), Earth's continuous oscillations observed on seismically quiet days, *Geophys. Res. Lett.*, *25*, 1553–1556, doi:10.1029/98GL01223.

Uchiyama, Y., and J. C. McWilliams (2008), Infragravity waves in the deep ocean: Generation, propagation and seismic hum excitation, *J. Geophys. Res.*, *113*, C07029, doi:10.1029/2007JC004562.

Watada, S., and G. Masters (2001), Oceanic excitation of the continuous oscillation of the Earth, *Eos Trans. AGU*, *82*(47), Fall Meet. Suppl., Abstract S32A-0620.

Webb, S. C. (1986), Coherent pressure fluctuations observed at two sites on the deep sea floor, *Geophys. Res. Lett.*, *13*, 141–144, doi:10.1029/GL013i002p00141.

Webb, S. C. (2007), The Earth's hum is driven by ocean waves over the continental shelf, *Nature*, *445*, 754–756, doi:10.1038/nature05536.

Webb, S. C. (2008), The Earth's hum: The excitation of Earth normal modes by ocean waves, *Geophys. J. Int.*, *174*, 542–566, doi:10.1111/j.1365-246X.2008.03801.x.

Webb, S. C., X. Zhang, and W. Crawford (1991), Infragravity waves in the deep ocean, *J. Geophys. Res.*, *96*, 2723–2736, doi:10.1029/90JC02212.

Y. Fukao, Institute for Research on Earth Evolution, Japan Agency for Marine-Earth Science and Technology, Natsushima-cho 2-15, Yokosuka, Kanagawa 237-0061, Japan. (fukao@jamstec.go.jp)

N. Kobayashi, Institute of Space and Astronomical Science, Japan Aerospace Exploration Agency, 3-1-1 Yoshinodai, Sagamihara, Kanagawa 229-8510, Japan. (kobayashi.naoki@jaxa.jp)

K. Nishida, Earthquake Research Institute, University of Tokyo, 1-1-1 Yayoi, Bunkyo, Tokyo 113-0032, Japan. (knishida@eri.u-tokyo.ac.jp)